Available online at www.sciencedirect.com

ScienceDirect

Energy Procedia 142 (2017) 661–666

Energy Procedia

www.elsevier.com/locate/procedia

9th International Conference on Applied Energy, ICAE2017, 21-24 August 2017, Cardiff, UK

An Up-scaling Strategy for Counter-flow Based Microfluidic Network: A Numerical Study

Xu Lu[a], Dennis Y.C. Leung[a], Yifei Wang[a], Huizhi Wang[b], Jin Xuan[b]*

[a]*Department of Mechanical Engineering, The University of Hong Kong, Pokfulam Road, Hong Kong*
[b]*Institute of Mechanical, Process and Energy Engineering, School of Engineering and Physical Sciences, Heriot-Watt University, Edinburgh, EH14 4AS, UK*

Abstract

This paper reports a computational demonstration and analysis of an innovative up-scaling counter-flow based microfluidic network to convert formic acid into electricity. This design consists of multi-dimensional T-shaped micro-scale channels that allow the inflow of liquid catholyte and anolyte from oppositely positioned inlets. It is revealed that the up-scaling strategy could effectively form primary and secondary counter-flow patterns, which are beneficial for high power output and fuel utilization at low flow rate operation. The design shows a breakthrough of the overall energy throughput and reactivity because of the full engagement of all available reaction sites. The energy loss mechanism introduced by the up-scaling network is also examined, demonstrating its performance intensification effect.

Peer-review under responsibility of the scientific committee of the 9th International Conference on Applied Energy.

Keywords: Fuel cell, Microfluidics, Up-scaling, Numerical simulation, Energy throughput

Nomenclature

E	equilibrium potential (V)	μ	viscosity (Pa s)	F	faradaic constant (C/mol)
ρ	density (kg/m^3)	g	gravitational acceleration (m/s^2)	σ	conductivity (S/m)
i	current density (A/m^2)	τ	the viscosity stress tensor (Pa)	η	activation overpotential (V)
j	mass flux (kg/m^2 · s)	χ	reaction order	u	velocity (m/s)
M	molar mass (g/mol)	φ	potential (V)	α	transfer coefficient
n	number of participating electrons	ω	mass fraction	γ	stoichiometric coefficients
n_t	number of electrons exchanged at the rate-limiting step	A	active area (cm^2)	S_i	production or consumption rate (kg/m^3 · s)
p	pressure (Pa)	V	voltage (V)	S_k	current source (A/m^3)

* Corresponding author. Tel.: +852 2859 7911; fax: +852 2858 5415.
E-mail address: ycleung@hku.hk.

1876-6102
Peer-review under responsibility of the scientific committee of the 9th International Conference on Applied Energy.
10.1016/j.egypro.2017.12.109

Subscript					
0	reference or boundary	i	species i	m	main reaction
ref	reference	a	anode	c	cathode
p	parasitic reaction				

1. Introduction

With its low-cost fabrication and mild operation condition, microfluidic fuel cell technology is regarded as a promising solution for portable electricity source. Most current research efforts on microfluidic fuel cells focus on the pattern that the laminar catholyte and anolyte streams flow in parallel[1]. Indeed, the natural mixing layer between the electrolytes could perform the same role as a physical barrier like a proton exchange membrane; however, keeping the characteristics of laminar flow requires continuous electrolyte supply into the microchannel, leading to considerable electrolyte wastage and low electrolyte utilization efficiency. To tackle this issue, this paper will employ a counter-flow design, which was firstly proposed to provide effective electrolyte separation in a vanadium redox flow battery with multiple vanadium oxidation states[2] and further developed as a formic acid fuel cell platform[3]. Figure 1(a) shows a schematic of the counter-flow pattern with air-breathing electrodes. The fuel, formic acid, is dissolved in the anolyte, which is supplied from the right-hand inlet and oxidized at the porous anode. Similarly, the catholyte is introduced from the left-hand inlet, providing a reaction site for the gaseous oxidant penetrating through the gas-diffusion anode. Unlike co-flow, the counter-flow pattern creates a chaotic mixing region and the dominant viscous effect stabilizes the interface, preventing the interaction between the fuel and oxidant. The diffusion transfer is suppressed by the opposite convection transfer and the diffusion time of reactive species is less than their convection time, i.e. residence time. In this way, only small electrolyte flow rate is required to form this virtual separating layer, allowing a high fuel utilization operation.

The economic feasibility is also a doubt on microfluidic electrochemistry in spite of the high area-specific performance. Its practicability is severely constrained by the low overall yield due to the inherent reactor size. Dimensional scale-out has been proven infeasible[4] due to the boundary layer growth and mixing layer perturbation accompanied by significant energy losses. Other efforts, such as two-cell planar array[5], vertical stack[6], multiplexing flow distribution[7], have suffered from low applicability to practical situations, where the fluid maldistribution is far more complex. Therefore, a new up-scaling path needs to be opened up for mass production and industrial application. This could be achieved based on the above-mentioned microfluidic platform, which has demonstrated by our group[8] and others[9] its capability for efficient system scale-out. Based on these genetic mechanisms, a microfluidic multi-dimensional modularization design will be proposed. Performance losses during the scale-out will be minimized by an effective liquid redistribution strategy. Two-dimensional shunt serpentine (Figure 1(b)) and up-scaling networks (Figure 1(c)) will then be numerically established.

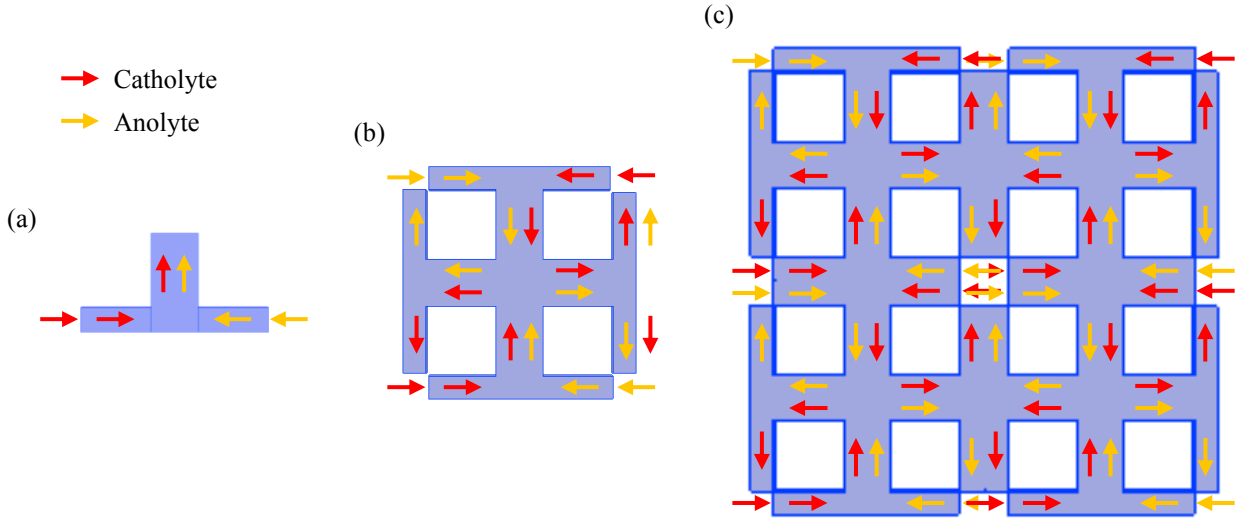

Figure 1. Schematics of counter-flow based fuel cell (a) unit, (b) module, and (c) up-scaling network.

2. Numerical Model

2.1 Basic assumptions

A finite element analysis software, COMSOL Multiphysics (COMSOL Group), is used to determine the flow pattern and electrochemical performance of the up-scaling network.

We make the following assumptions and simplifications during the calculation:

- The system is isothermal and at steady-state. This is a reasonable assumption for an electrochemical cell with a flowing electrolyte;
- The electrolyte is an incompressible Newtonian fluid and the flow is laminar;
- Gas is weakly compressible and the flow in the gas channel is laminar;
- The side walls of the cell are impermeable and the slip is zero;
- Concentrations do not vary along the cell cross section, as we enforce slip and zero species flux at the left and right walls of the cell;
- The fluid's properties, including density and viscosity, are not influenced by the solute concentration.

2.2 Microfluidic characterization

Reynolds number, used to verify the microfluidic characteristics of the geometry, is defined as:

$$\mathrm{Re} = \frac{\rho v L'}{\mu} \quad \text{Equ. (1)}$$

where L' is the characteristic length (hydraulic diameter).

2.3 Hydrodynamics

For a microfluidic network, continuity equation, conservation equation of species, and the steady state Navier-Stokes equation are applicable without the problematic convective term:

$$\nabla \cdot (\rho u) = 0 \quad \text{Equ. (2)}$$

$$\nabla \cdot (\rho \omega_i u) = -\nabla \cdot j_i + S_i \quad \text{Equ. (3)}$$

$$\nabla p = -\rho u \cdot \nabla u + \mu \nabla^2 u + \rho g \quad \text{Equ. (4)}$$

where the density of formic acid solution is fitted according to literature[3]:

$$\rho = 1011 + 208 \cdot w_f \quad \text{Equ. (5)}$$

2.4 Mass transfer

Maxwell Stefan expression is used to describe the diffusive transport. The mass-balance equations for the solute are:

$$j_i = -(\rho D_i \nabla w_i + \rho w_i D_i \frac{\nabla M_n}{M_n} \quad \text{Equ. (6)}$$

$$M_n = (\sum_i \frac{w_i}{M_i})^{-1} \quad \text{Equ. (7)}$$

The situation where the viscosity depends quadratically on the concentration occurs in solutions of macromolecules. For H_2SO_4, it can be assumed that a change in solute concentration does not influence the fluid's density and viscosity. This implies that it is possible to first solve the Navier-Stokes equations and then solve the mass balance equation. As the Peclet number of the present system is greatly larger than 1, it is necessary to maintain numerical stability when solving the Fick's equation. COMSOL automatically includes the stabilization by default, so no explicit settings will be required.

2.5 Kinetics and overpotentials

The cathode reaction, which is also the anode parasitic reaction, is:

$$2HCOOH \rightarrow 2CO_2 + 4H^+ + 4e^- \quad \text{Equ. (8)}$$

The anode, which is also the cathode parasitic reaction, is:

$$O_2 + 4H^+ + 4e^- \rightarrow 2H_2O \quad \text{Equ. (9)}$$

The parasitic current is considered as it could significantly affect the cell performance due to fuel crossover.

The electrochemical kinetics for the main and parasitic reactions is governed by Butler-Volmer equation, where the oxidant crossover could be neglected because of the low solubility of gaseous oxygen:

$$i_c = i_{0,c}\left(\frac{c_0}{c_{0,ref}}\right)^{\chi}\left(e^{\frac{\alpha_a n_t F \eta}{RT}} - e^{\frac{-\alpha_c n_t F \eta}{RT}}\right) + i_{0,a}\left(\frac{c_f}{c_{f,ref}}\right)^{\chi}\left(e^{\frac{\alpha_a n_t F \eta}{RT}} - e^{\frac{-\alpha_c n_t F \eta}{RT}}\right) \quad \text{Equ. (10)}$$

$$i_a = i_{0,a}\left(\frac{c_f}{c_{f,ref}}\right)^{\chi}\left(e^{\frac{\alpha_a n_t F \eta}{RT}} - e^{\frac{-\alpha_c n_t F \eta}{RT}}\right) \quad \text{Equ. (11)}$$

$$\eta = \varphi_s - \varphi_l - E \quad \text{Equ. (12)}$$

The sink and source of reactant species are:

$$S_i = M_i \frac{\gamma_i \nabla \cdot i}{n_i F} \quad \text{Equ. (13)}$$

where $-\sigma\Delta\varphi = \nabla \cdot i$ relating potential and current.

2.6 Boundary conditions

The boundary conditions are prescribed in Table 1 below:

Table 1. Boundary conditions.

Position	Condition
Inlet	constant species mass fraction constant inlet velocity
Outlet	zero-diffusive flux of species constant outlet pressure
Electrodes	non-flux boundaries
Wall	non-slip condition
Solution phase	non-flux boundaries everywhere constant potentials at the electrodes

The key input parameters of the model are summarized in Table 2.

Table 2. Key parameters of the model.

Parameter	Meaning	Value
L'	hydraulic diameter	0.28 mm
μ	fluid viscosity	$1\ \mathrm{mPa \cdot s}$
ν	characteristic velocity for Reynolds number calculation	$0.135\ \mathrm{m/s}$
ρ	electrolyte density	$1000\ \mathrm{kg/m^3}$
Re	Reynolds number	0.0378
$c_{f,ref}$	reference fuel concentration	1000 mol/L
$c_{f,ref}$	reference oxidant concentration	1.25 mol/L
c_0	oxidant concentration	0.25 mol/L
i_a	exchange current density of anode	$0.004\ \mathrm{A/m^2}$
i_o	exchange current density of cathode	$0.06\ \mathrm{A/m^2}$
T	temperature	298K
χ		1
α_a	anodic transfer coefficient	0.5
α_c	cathodic transfer coefficient	0.5
n_t		1
D_f	diffusion coefficient	$1.6 \times 10^{-8}\ \mathrm{m^2/s}$

3. Results and Discussions

In this simulation the maximum Re is 0.0378, which is far less than 1. The low Reynolds number indicates that the electrolytes would flow laminarly through the micro-channels; however, fuel crossover may still happen in the chaotic mixing regime of a counter-flow based cell due to the overwhelming convection over diffusion. Therefore, it is necessary to evaluate the interfacial mixing patterns of the up-scaling network to prove the effectiveness of the concept. At low flow rate region (Figure 2(a-c)), i.e. $<1000\ \mu\mathrm{L/min}$, the mixing layer thickness decreases with higher flow rates and no pressure-driven secondary counter-flow is generated at the cross zone (Figure 2(a-2)). This is because of the pressure loss along the primary inlet channel.

This trend gets reversed beyond the flow rate of $1000\ \mu\mathrm{L/min}$ for the unit cell. More and more clearly observable disturbances could be found at the mixing layer (Figure 2(d1-g1)) and become significantly perturbative at $2500\ \mu\mathrm{L/min}$. Meanwhile, at the same flow rate region, higher flow rates start enabling the formation of secondary counter-flow pattern, which could be better illustrated by plotting the mass fraction distribution maps of the electrolyte (Figure 2(d4-g4)), i.e. sulfuric acid solution. This phenomenon is resulted from the fact that in an up-scaling network, the excessive pressure drop and consequent strong convection transfer would be relieved to fill in the 'pressure vacuum' cross zone, creating a secondary driven force for the secondary convection transfer to suppress the diffusion transfer.

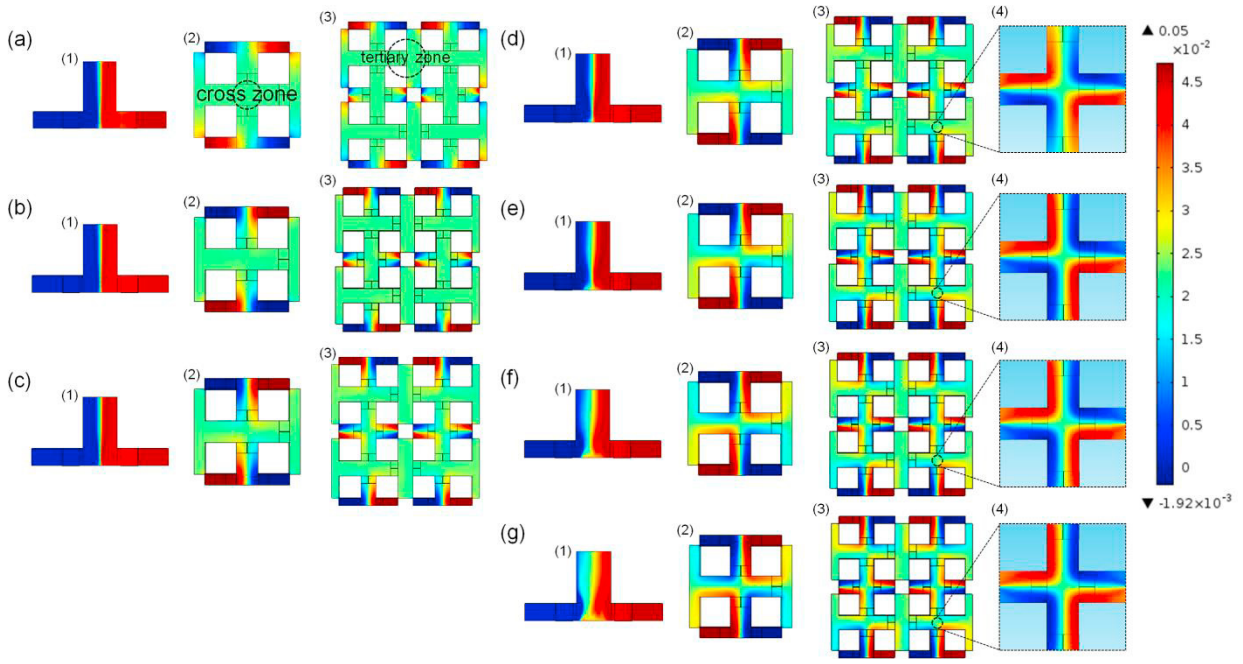

Figure 2. Mass fraction distribution maps of formic acid obtained at flow rates of (a) 100, (b) 500, (c) 1000, (d) 1500, (e) 2000, (f) 2500, and (g) 3000 μL/min from (1) unit, (2) module, and (3) up-scaling network. (4) Electrolyte mass fraction distribution maps at the cross zone.

The effect of flow rates on the performance of reactors at different scales is also examined. The transverse comparison across flow rates demonstrates its insignificant influence on unit cell (Figure 3(a)) as the anolyte and catholyte are always well separated even with the strong interferential convection at high flow rates. On the other hand, the electrochemical performance of a module (Figure 3(b)) and up-scaling network (Figure 3(c)) is slightly improved with flow rates increasing, reflecting the engagement of the secondary counter-flow pattern at the cross zone. The longitudinal comparison across reactor scales shows significant advancement of the reactivity by scaling out (Figure 3(d)). Near the peak power density regime, i.e. output voltage ~0.2V, the current density output by a unit cell is ~20 mA/cm^2, whilst that of a module or up-scaling network is kept at ~25 mA/cm^2. The limiting current density of the up-scaling network (~180 mA/cm^2) is more than twice as much as that of a unit cell (~70 mA/cm^2). This validates the formation and effectiveness of the secondary counter-flow pattern, which doubles the reactive area to collect and harvest the waste convection energy.

An up-scaling network is actually 4 modules that are electrically in parallel and a module consists of 4 unit cells. Considering a single electrode area of L=W=1 mm, there are 1, 4, and 20 coupled reactive sites in a unit, module and up-scaling network. It should also be noted that there are 4 more coupled sites in an up-scaling network than linear multiple because tertiary counter-flow would be formed at the inter-connection zone of adjacent modules (Figure 2(a-3)). Therefore, the overall peak power density output of a unit, module and up-scaling network are 0.04, 0.28 and 1.33 mW, respectively and could be linearly increased by further stacking.

Numerical data also show a slight limiting reactivity decrease of the higher scale network (~175 mA/cm^2 vs. ~185 mA/cm^2). This implied an up-scaling efficiency of 95% in an ideal condition. Taking fictional loss and uneven pressure distribution into account for practical experiment, a target of 85% up-scaling efficiency could be set up.

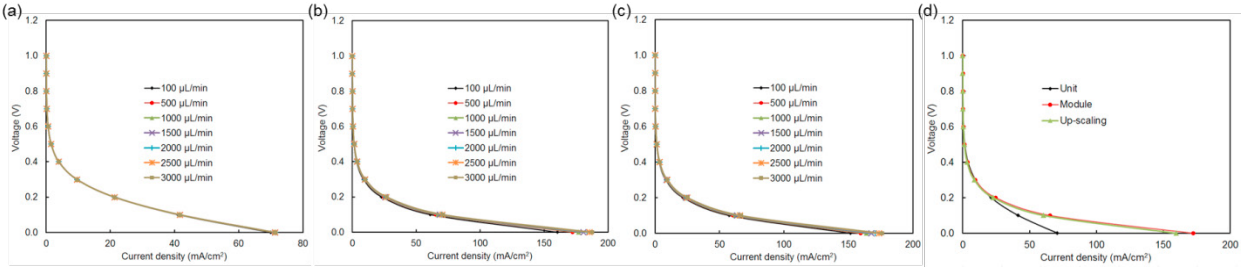

Figure 3. Polarization curves obtained from (a) unit, (b) module, (c) up-scaling network at different flow rates, and (d) longitudinal comparison of the polarization across reactor scales at flow rates of 500 μL/min.

4. Conclusion

Manipulation of the overall throughput in microfluidic fuel cell is of great importance to approach the economic feasibility. This work proposed and demonstrated an innovative up-scaling strategy for counter-flow based microfluidic network. The microfluidics and diffusive flow were monitored and characterized. The up-scaling design benefited from the separation of the reactive sites, which facilitated the formation of secondary counter-flow pattern and doubled the electrode area. The effect of hydrodynamic condition suggested a better manipulation of the flow behaviors by utilizing the excessive pressure at the cross zone in an up-scaling network. As a result, a significantly improved upper bound of current density was observed. This unique operation mode could be further developed to optimize the reactivity, fuel utilization and interfacial mixing layer without sacrificing the limitation. Experimental verification is currently conducted to validate the concept and fine tune the model. To our best knowledge, rare similar attempts have been reported in literature and this study opens up a new direction for microfluidic fuel cell research.

Acknowledgement

This project is financially supported by the CRCG of the University of Hong Kong and the Scottish – Hong Kong SFC/RGC Joint Research Scheme XHKU710/14 and SFC Project H15009.

Reference

[1] Kjeang E, Djilali N, Sinton D. Microfluidic fuel cells: A review. Journal of Power Sources. 2009;186:353-69.
[2] Salloum KS, Posner JD. Counter flow membraneless microfluidic fuel cell. Journal of Power Sources. 2010;195:6941-4.
[3] Xu H, Zhang H, Wang H, Leung DY, Zhang L, Cao J, et al. Counter-flow formic acid microfluidic fuel cell with high fuel utilization exceeding 90%. Applied Energy. 2015;160:930-6.
[4] Kjeang E, Proctor BT, Brolo AG, Harrington DA, Djilali N, Sinton D. High-performance microfluidic vanadium redox fuel cell. Electrochimica Acta. 2007;52:4942-6.
[5] Salloum KS, Posner JD. A membraneless microfluidic fuel cell stack. Journal of Power Sources. 2011;196:1229-34.
[6] Moore S, Sinton D, Erickson D. A plate-frame flow-through microfluidic fuel cell stack. Journal of Power Sources. 2011;196:9481-7.
[7] Cohen JL, Westly DA, Pechenik A, Abruna HD. Fabrication and preliminary testing of a planar membraneless microchannel fuel cell. Journal of Power Sources. 2005;139:96-105.
[8] Wang H, Gu S, Leung DY, Xu H, Leung MK, Zhang L, et al. Development and characteristics of a membraneless microfluidic fuel cell array. Electrochimica Acta. 2014;135:467-77.
[9] Elvira KS, i Solvas XC, Wootton RC. The past, present and potential for microfluidic reactor technology in chemical synthesis. Nature chemistry. 2013;5:905-15.